

Direct evidence of hidden local spin polarization in a centrosymmetric superconductor $\text{LaO}_{0.55}\text{F}_{0.45}\text{BiS}_2$

Shi-Long Wu¹, Kazuki Sumida², Koji Miyamoto¹, Kazuaki Taguchi², Tomoki Yoshikawa², Akio Kimura², Yoshifumi Ueda¹, Masashi Arita¹, Masanori Nagao³, Satoshi Watauchi³, Isao Tanaka³ & Taichi Okuda^{1*}

¹Hiroshima Synchrotron Radiation Center (HSRC), Hiroshima University, 2-313 Kagamiyama, Higashi-Hiroshima 739-0046, Japan

²Graduate School of Science, Hiroshima University, 1-3-1 Kagamiyama, Higashi-Hiroshima 739-8526, Japan

³Center for Crystal Science and Technology (CCST), University of Yamanashi, 7-32 Miyamae, Kofu, Yamanashi 400-8511, Japan

Abstract

Conventional Rashba spin polarization is caused by the combination of strong spin-orbit interaction (SOI) and spatial inversion asymmetry. However, Rashba- and Dresselhaus-type spin-split states are predicted in LaOBiS_2 system by recent theory even though the crystal structure is centrosymmetric, which stem from the local inversion asymmetry of active BiS_2 layer. By performing high-resolution spin- and angle-resolved photoemission spectroscopy, we have investigated the electronic band structure and spin texture of superconductor $\text{LaO}_{0.55}\text{F}_{0.45}\text{BiS}_2$. Our studies present direct spectroscopic evidence for the local spin polarization in the vicinity of X point of both valence band and conduction band. Especially the coexistence of Rashba-like and Dresselhaus-like spin textures has been observed in the conduction band for the first time. The finding is of key importance for fabrication of proposed dual-gated spin-field effect transistor (SFET). Moreover, the spin-split band leads to a spin-momentum locking Fermi surface from which novel superconductivity emerges. Our demonstration not only expands the scope of spintronic materials but also enhances the understanding of SOI related superconductivity.

According to the well-known Kramers theorem, spatial inversion symmetry $E(\mathbf{k}, \uparrow) = E(-\mathbf{k}, \uparrow)$ and time-reversal symmetry $E(\mathbf{k}, \uparrow) = E(-\mathbf{k}, \downarrow)$ result in $E(\mathbf{k}, \uparrow) = E(\mathbf{k}, \downarrow)$, guarantee the electronic states of non-magnetic centrosymmetric materials must be spin degenerate. Namely, a momentum-dependent spin-split state usually comes from global inversion asymmetry of system. For instance, conventional Dresselhaus effect (denoted as D-1 in ref. 1) can derive from non-polar bulk crystal with inversion asymmetry^{2,3}. Alternatively, polar bulk materials⁴ or surface or interface under electrostatic potential gradient leads to conventional Rashba effect (denoted as R-1)⁵⁻⁸. However, recent theoretical formalism reconstructed the traditional Rashba and Dresselhaus effects in atomic scale¹. Microscopically, atomic site that belongs to a non-centrosymmetric point group can carry either a local dipole field or site inversion asymmetric crystal field, inducing local Rashba

effect (denoted as R-2) or local Dresselhaus effect (denoted as D-2), respectively⁹.

The theoretical works suggested that LaOBiS₂ and the related compounds can be such a system possessing R-2 and/or D-2 due to the breaking of local inversion symmetry in each BiS₂ bilayer and the opposite polar fields caused by ionic bonding between (BiS₂)-bilayer and (La₂O₂)²⁺ layer as indicated in Fig. 1a. Since the projected local spin polarization on each real-space sector of BiS₂ bilayer in LaOBiS₂ crystals holds opposite orientation, so called spin-layer locking effect, has been theoretically predicted in the LaOBiS₂ film at first⁹ which could offer advantages for the design of new generation of spin-field effect transistors (SFET)¹⁰. Theoretical study of either film⁹ or bulk LaOBiS₂¹ further pointed out that spin texture of conduction band at each X point in Brillouin zone must be non-helical originating from D-2 effect whereas the valence band possesses helical spin texture originating from R-2 effect.

Moreover, with electron doping by substitution of oxygen with fluorine, LaO_{1-x}F_xBiS₂ is manifested as one of BiS₂-based superconductors with similar properties of cuprate superconductors such as rather high value of $2\Delta/k_B T_C$ ¹¹ and Cooper pairing symmetry¹². The system exhibits the maximum superconducting critical temperature (T_C) of 10.6 K at $x \sim 0.5$ ¹³ among all the BiS(Se)₂ based superconductors, hence serves an excellent platform to combine superconductivity with local Rashba effect, by which we focus on a new approach to study the mechanism of Cooper pairing. Note that, heretofore, Rashba superconductors¹⁴⁻¹⁷ with mixed singlet and triplet pairings have been limited to non-centrosymmetric compounds or surface systems.

Intriguingly, recent theoretical papers proposed that BiS₂-based superconductors could be classified as time-reversal invariant (TRI) weak topological superconductor (TSc) as a result of combination of possible $d^*_{x^2-y^2}$ pairing symmetry and possible spin-split electronic band at X points^{18,19}. Therefore BiS₂-based superconductors may have a dominant triplet pairing component arising from the spin-orbit interaction (SOI) and respecting time-reversal symmetry. Consequently the dominant triplet gap can cause gap sign changes between the spin-split Fermi pockets^{18,19} which give rise to weak topological superconductivity²⁰. The evidence of spin-polarized states caused by SOI and breaking of local inversion symmetry on LaOBiS₂ or family compounds (LaOBiSe₂, etc.), however, has not yet been reported so far.

In this letter, we provide the direct evidence for the hidden local spin polarization in the vicinity of time-reversal invariant momenta (TRIM) X points of both conduction band (CB) and valence band (VB) in LaO_{0.55}F_{0.45}BiS₂ superconductor by high-resolution spin- and angle-resolved photoemission spectroscopy (SARPES). Especially the conversion from Rashba-like to Dresselhaus-like spin texture at some k-point has been directly observed in the conduction band. Our observation of the unconventional spin-split state in LaO_{0.55}F_{0.45}BiS₂ not only promotes BiS₂-based materials as an important platform for realizing spintronic devices but also enhances the understanding of SOI related superconductivity.

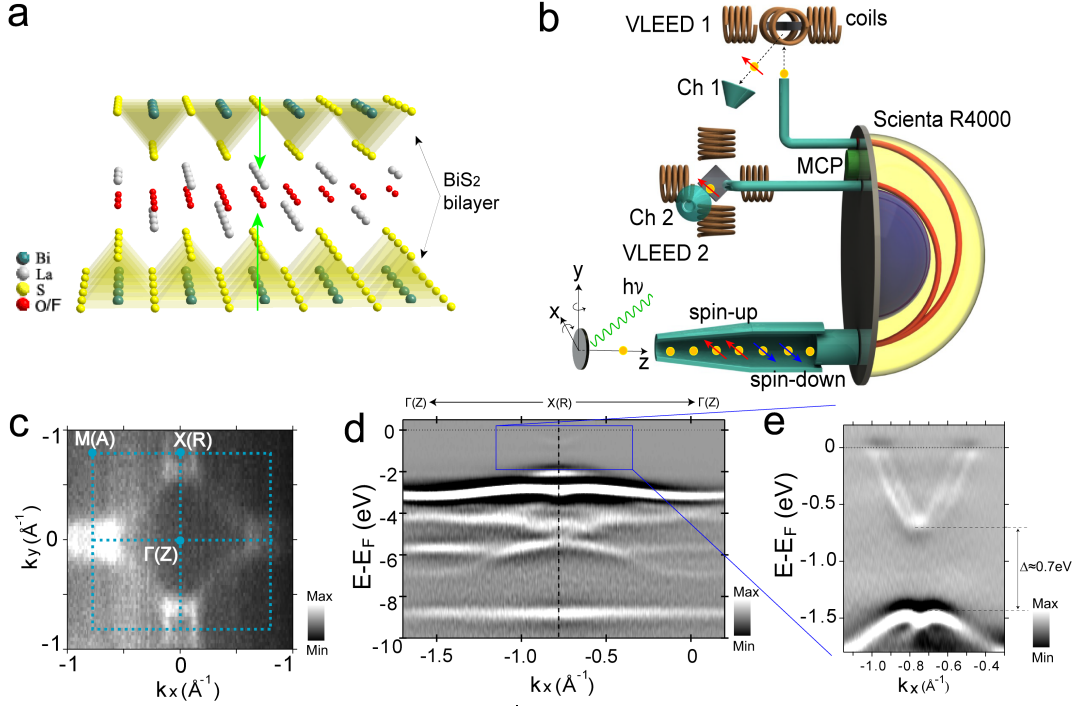


Figure 1 | Electronic structure observation of $\text{LaO}_{0.55}\text{F}_{0.45}\text{BiS}_2$ by angle resolved photoemission (ARPES). (a) Crystal structure of $\text{La}(\text{O},\text{F})\text{BiS}_2$ with a buffer layer $\text{La}(\text{O},\text{F})$ separating the active BiS_2 bilayer. Green arrows denote opposite local polar fields in BiS_2 bilayer. (b) Illustration of Efficient SPin RESolved SpectroScOpy (ESPRESSO) machine at HiSOR and the experimental geometries for the ARPES and spin-ARPES measurements. (c) Constant energy contour (CEC) at $E_B=0.2$ eV. (d) Band structure (E - k map) along $\Gamma(\text{Z})$ - $\text{X}(\text{R})$ obtained by ARPES measurement was taken with $h\nu=70$ eV and $T_S=50$ K. The CEC map is integrated over a window of ± 20 meV and the E - k map is obtained by the second derivative of energy distribution curves (EDCs) of original ARPES data. (e) Bands in the range of 0-1.8 eV below Fermi level (the boxed area of Fig. 1d) are clearly seen in the ARPES data taken with $h\nu=18$ eV and $T_S=50$ K.

Figure 1a shows the crystal structure of $\text{LaO}_{1-x}\text{F}_x\text{BiS}_2$ possessing a P4/nmm symmetry with an inversion center located at the center of two nonequivalent O atoms, stacked alternatively an active BiS_2 bilayer and a buffer $\text{La}(\text{O},\text{F})$ layer^{13,21-23}. The green arrows in Fig. 1a show the dipole fields along normal direction of BiS plane induced by ionic bonding between $(\text{BiS}_2)^-$ bilayer and $(\text{La}_2\text{O}_2)^{2+}$ layer.

Figure 1c shows the constant energy contour (CEC) map of $\text{LaO}_{0.55}\text{F}_{0.45}\text{BiS}_2$ grown by flux method²⁴ at binding energy (E_B) of 0.2 eV taken with ESPRESSO machine^{25,26} (Fig. 1b) (see Methods section below for more detailed information). Rectangle-like Fermi pocket locates around each X symmetry point in the Brillouin zone, reflecting the four-fold symmetry of crystals. Fig. 1d shows the band structure along $\Gamma(\text{Z})$ - $\text{X}(\text{R})$ (Γ -X for short) high-symmetry direction obtained by $h\nu=70$ eV. In accordance with the previous density functional theory (DFT) calculations^{27,28}, several states from 2 to 6 eV below Fermi level (E_F) are observed in valance band, which are attributed mainly to the 2p states of O and S atoms. Although the intensity of highest valance band (HVB) and lowest conduction band (LCB), which shift below E_F by fluorine doping, is relatively weak in the boxed area of Fig. 1d, it is quite clear in Fig. 1e taken with $h\nu=18$ eV. The splitting electron-like conduction band crosses E_F around X point coming from Bi-6p state^{27,28}, so that the BiS plane dominantly contributes to the electronic conduction. Figs. 1d and 1e also show that, along the Γ -X direction, the maximum value of valance band is at the X point with a bandgap of about 0.7 eV to the bottom of the conduction band being consistent with the band calculation²⁸. We note the overall features of electronic structure in Figure 1 are in good

accordance with previous calculations and experiments^{1,10,28} for the bulk electronic states in BiS₂-based compounds.

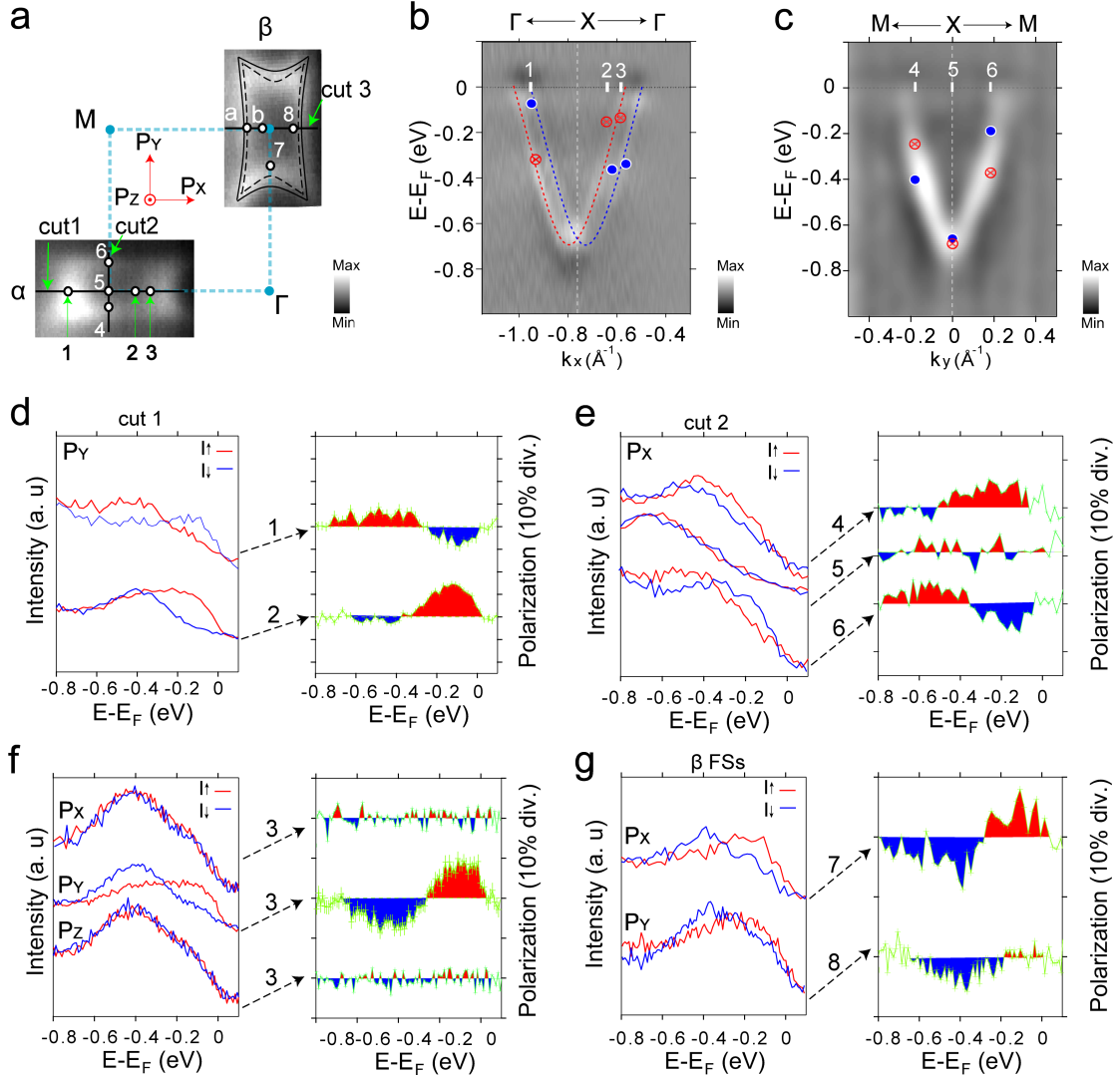


Figure 2 | Spin- and angle-resolved photoemission spectroscopy (SARPES) of LCB. (a) Fermi surface sheets (FSs) labeled α and β of LCB measured by using photon energy of 18 eV and the comparison with DFT calculation of FSs (black lines). The CEC maps are integrated over a window of ± 20 meV. The dots around "X" point denote the momentum points where we performed spin measurements, the points "1" to "3" along cut 1 and the points "4" to "6" along cut 2 were also marked in Figs. 2b and 2c. Coordinate axes (P_x , P_y , P_z) denote positive directions of spin vectors. (b) Band dispersion measured by ARPES ($h\nu=18$ eV) along the cut 1 (Γ -X- Γ line, second derivative). The dashed red and blue lines represent extracted positions from the EDCs used for the estimation of Rashba parameter. (c) The same as (b) but along the cut 2 (M-X-M line, second derivative). (d) Spin-resolved EDCs of P_y along cut 1. Right panel shows the corresponding spin polarizations. (e) The same as (d) but of P_x along cut 2. The peak positions of spin-up and spin-down states along cut 1 and cut 2 are indicated in (b) and (c) by red crosses and blue dots. (f) The same as (d) but of P_x , P_y and P_z at point "3". (g) The same as (d) but of P_x at point "7" and P_y at point "8".

In Figure 2 we present more detailed band structure obtained by ARPES measurement with $h\nu=18$ eV around X symmetry point. Fig. 2a shows CEC images at the Fermi level (*i.e.* Fermi surface sheets (FSs)) and the calculated FSs for LaO_{1-x}F_xBiS₂ ($x \sim 0.45$) (black lines) plotted from previous studies^{12,28} for comparison. The rectangle-like shape and its size are corresponding to doping level of ~ 0.45 in LaO_{1-x}F_xBiS₂ system. Fig. 2b shows the splitting LCB along Γ -X- Γ line (cut 1 in Fig. 2a). In contrast to Fig. 2b, the LCB along M-X-M line (cut 2) does not show clear band splitting which is consistent with the expected smaller splitting along the direction by the DFT calculation¹.

Given that pure Rashba-type spin polarized HVB as well as the LCB in LaOBiS₂ system, namely assuming that the band splitting from Fig. 1e (Fig. 2b) is due to Rashba spin-orbit interaction (RSOI), we can estimate that the Rashba energies $E_R = \hbar^2 k_R^2 / 2m^*$ (k_R describes the shift between band extremum and crossing, m^* denotes the effective mass) are 24 meV for LCB and 45 meV for HVB. Since the corresponding momentum offsets $k_R = \alpha_R m^* / \hbar^2$ are 0.04 Å⁻¹ and 0.08 Å⁻¹, we can evaluate the Rashba parameters $\alpha_R = 2E_R / k_R = 1.20$ eV·Å and 1.13 eV·Å for LCB and HVB, respectively. The magnitudes of the Rashba parameter for HVB is a little smaller than predicted value 1.84 eV·Å for HVB¹⁰.

In order to investigate the real origin of the splitting in LCB and HVB we have performed SARPES measurement utilizing the function of three-dimensional spin-vector analysis of ESPRESSO machine²⁶ at the representative momentum points marked by white dots in Fig. 2a. Figs. 2d-g show the SARPES results of LCB at several momentum points around “X” with 3D spin-vector analysis. Fig. 2d illustrates the spin resolved energy distribution curves (spin-EDCs) of P_Y (=tangential spin to the Fermi surface) at the momentum positions “1” and “2” along Γ -X- Γ line (cut 1). In the figure, the red (blue) lines denote spin-up (spin-down) states. The definition of positive directions of spin vectors are shown with the coordinate axes in Fig. 2a. The results indicate that the LCB is unambiguously spin polarized and the spin-splitting occurs at each measuring momentum position. Moreover, the spin reversal can be observed on opposite sides of “X” point. Namely, the sign of spin polarizations at position “1” is opposite to that of position “2” in the spin-resolved EDC spectra.

In contrast with the obvious spin polarization of P_Y , spin polarizations of P_X and P_Z are negligible at position “3” as shown in Fig. 2f indicating the spin polarization is mainly along in-plane tangential direction of Fermi surface. To further clarify the spin texture of the whole FSs we have also performed spin measurement of P_X (=tangential spin to the Fermi surface) at positions “4”, “5” and “6” along M-X-M line (cut 2) by tilt rotation of sample. The almost identical spectra in opposite spin channels of P_X at position “5” (*i.e.* at the X(R) high symmetry point) confirm the spin degeneracy of LCB at the time-reversal invariant momenta (TRIM). Although the band splitting is not obvious in normal ARPES measurement in Fig. 2c, clear spin polarizations and its reversal with respect to X symmetry point are also confirmed in the M-X-M line as shown in the Fig. 2e. The peak positions of spin-resolved EDCs in Fig. 2d and 2e are plotted in Fig. 2b and 2c with several marks (*i.e.* dots and crosses) being in reasonable agreement with the observed band dispersions by normal ARPES measurement. The observed spin reversals of P_X along M-X-M line and P_Y along Γ -X- Γ line indicate the overall counter-helical spin texture for LCB, which strongly suggests that Rashba spin polarization occurs in LCB.

On the other hand, it is also known that various experimental geometries such as changes of incident angle of synchrotron-radiation (SR) light, photon energy and so on could affect the observed spin polarization especially in the system with strong SOI²⁹. Thus, to make a double check of our results, we have performed similar measurement in β slice of FSs. In addition, with comparison of measurements of α and β slices we can not only confirm the Rashba-type spin polarization but also investigate the spin texture of FSs in the whole Brillouin zone. Fig. 2g shows the spin-resolved EDC spectra and their spin polarizations at positions “7” and “8” in β FSs. Clear spin polarizations and its sign of P_X at position “7” and P_Y at position “8” again confirm the helical spin texture around X symmetry point in β FSs. In other words, the directions of polarizations at positions “7” and “8” are equivalent to those of positions “4” and “3”, respectively. As a result, the LCB around each high symmetry X point in Brillouin zone has the same counter-helical spin

texture.

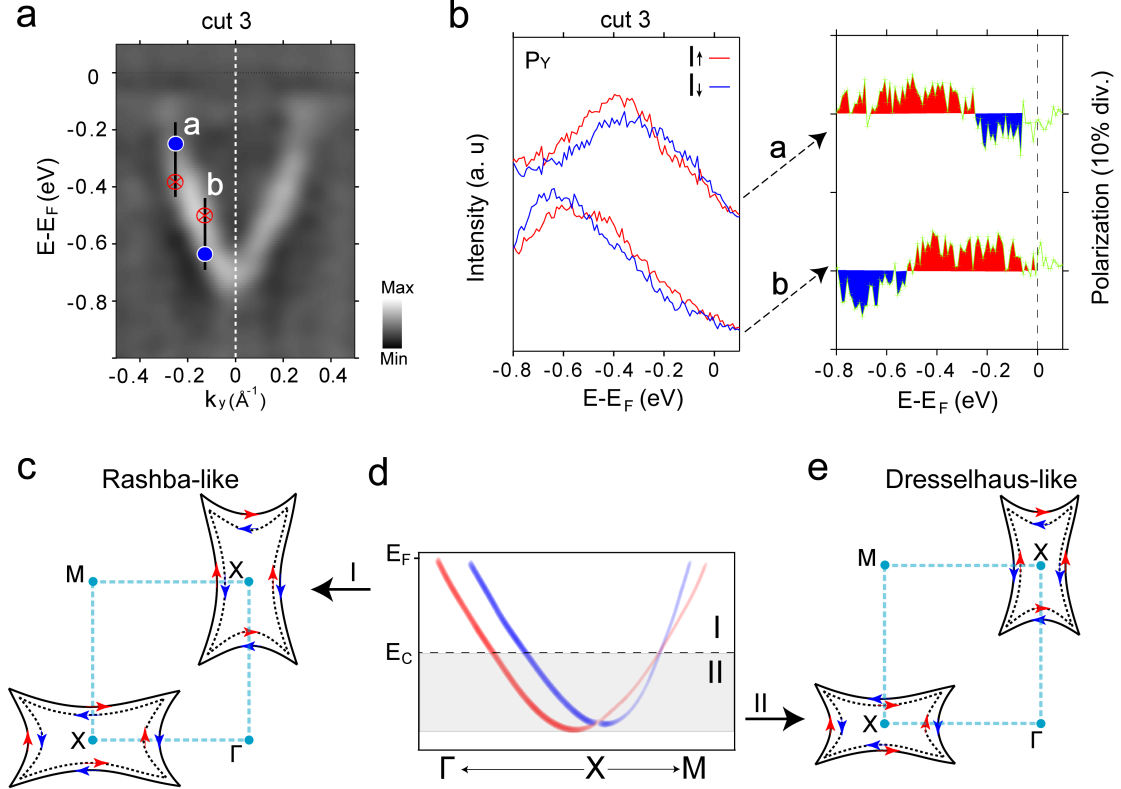


Figure 3 | Summary of the observed conversion of Rashba-like and Dresselhaus-like spin textures for LCB. (a) Band dispersion measured by ARPES ($h\nu=18$ eV) along the cut 3 in Fig. 2a (X-M line). (b) Spin-resolved EDCs of P_γ at "a" and "b" points in Fig. 2a, right panel shows the corresponding spin polarizations. The peak positions of spin-resolved EDCs are indicated with crosses and dots in (a). The reversal of spin polarizations at "a" and "b" points leading to a different spin textures (Rashba-like and Dresselhaus-like) in LCB. (c) The Rashba-like spin texture of the rectangle-like shape FSs at upper part of LCB (region I in Fig. 3d). (e) The Dresselhaus-like spin texture of CECs at lower part of LCB (region II in Fig. 3d) derives from the crossing of spin-polarized LCB at $E=E_c$ along X-M line which was taken from Refs. [1,10] and schematically indicated in (d). The red and blue colors for arrows and energy bands represent spin-up and down states, respectively.

Therefore, SARPES measurement confirmed that each slice of rectangle-like FSs has a counter-helical spin texture as summarized in Fig. 3c. Furthermore, the Rashba-like counter-helical spin texture, being consistent with the theoretical prediction, is also strongly suggested in HVB by our SARPES measurement (see Fig. S3 of supplementary information).

However, we must confirm the bulk contribution in the observed rectangle-like shape FSs so as to conclude that the counter-helical spin texture is attributed to local Rashba effect (R-2 effect) instead of surface Rashba spin splitting (R-1 effect). Recently bulk sensitive soft X-ray ARPES using photon energy of 880 eV was performed with $\text{LaO}_{0.54}\text{F}_{0.46}\text{BiS}_2$ crystal²⁸, which concluded that the observed rectangle-shape FSs by VUV-ARPES with 70 eV is the contribution of bulk state because of the close similarity of FSs between 880 eV and 70 eV measurement which is almost identical to the one obtained with 18 eV in our experiment. In addition, the overall agreement between calculated bulk band structures and experimentally observed band dispersions also strongly suggests that the observed LCB band is bulk state of $\text{LaO}_{0.55}\text{F}_{0.45}\text{BiS}_2$ crystal. Therefore, we believe that the observed spin polarization at LCB is attributed to local Rashba effect (R-2). The reason why we can extract the spin polarization by local Rashba effect by photoemission is probably due to the short mean free path of the photoemission measurement using low energy photon as demonstrated in WSe_2 system recently^{10,30}.

At a first glance, nevertheless, our observation of Rashba-type spin texture in LCB is

being inconsistent with the theoretical prediction in which the Dresselhaus-type spin texture was expected for the LCB¹. As indicated in Fig. 3d, in the theory paper, band crossing is predicted along X-M line which divides LCB into upper and lower parts (regions I and II) in LaOBiS₂ compound^{1,9,10} such that the lower LCB has non-helical spin texture whereas the upper LCB possesses helical spin texture suggesting the coexistence of D-2 and R-2 spin polarizations (see Fig. S2 of supplementary information). In order to investigate the novel phenomenon we have performed further SARPES observation very near to the X point along X-M line as in Fig. 3a and 3b. Intriguingly, we found that the spin polarization close to the X point is opposite to that of momentum position further from the X point strongly suggesting the transition from Dresselhaus-like to Rashba-like spin texture with varying binding energy. Therefore our observation is in good agreement with previous theoretical prediction though the crossing point seems to be a little nearer to the X point in the experiment than theoretical prediction.

From the application point of view, our finding of spin-active BiS₂ bilayer opens the pathway to realize the LaOBiS₂-based fast SFET. Since the opposite spin polarizations lock with BiS₂ bilayer, it is much easier to select a different layer so as to obtain reversal spin-polarized state via applying a small electric field⁹. Further exploration of local spin-polarization on iso-structural materials such as LaOBiSe₂³¹, (LaO)₂(SbSe₂)₂³² and so on will play an essential role in fabrication of spintronic devices.

Finally, we would briefly discuss the relationship between the local Rashba spin polarization and superconductivity. R-2 spin polarization corresponds to upper LCB near the Fermi level as shown in Fig. 3c such that the spin-momentum locking Fermi surface could have profound effects on the emergence of superconductivity in La(O,F)BiS₂. There is a broaden range of literatures to address unconventional superconductivity with inversion asymmetry in non-centrosymmetric heavy fermion compounds¹⁴⁻¹⁷. Because the broken inversion symmetry induces RSOI, as a result, different parities, spin-singlet and spin-triplet pairing, can be mixed in a superconducting state. Our experimental results evidently demonstrate the superconducting BiS₂ layers are also spin-active, thereby singlet and triplet pairings can be mixed in the wave function of the Cooper pairs^{14,15,16}. These observations may suggest a new approach to enhance superconducting critical temperature (T_c) by increasing strength of RSOI in the BiS₂-based system¹⁷. Furthermore, it is suggested that the spin-active layers can have nontrivial topology if the superconducting gap wavefunction has opposite signs on the spin-momentum locking Fermi surface^{18,19,20}. The local spin polarization of electron pockets directly observed in present study acts as an essential ingredient, could lead to intrinsic topological superconductivity in the BiS₂-based system.

In conclusion, we have found that SOI plays a significant role in the electronic energy bands of centrosymmetric superconductor LaO_{0.55}F_{0.45}BiS₂ with globally centrosymmetric crystal structure. Using high-resolution spin- and angle-resolved photoemission spectroscopy, we directly observed the local Rashba and Dresselhaus spin polarization in a superconductor for the first time. Since the spin-split Fermi pockets demonstrated by present experiment could have significant effects on Cooper paring and topological properties, we expect further works in BiS₂-based systems can promote studies of topological superconductors (TSc) and Marjorana fermions. Therefore, not only the result is of key importance for applying these compounds to SFET, but also offers an accessible paradigm to probe, manipulate bulk spin polarization based on local asymmetry and search

TSc on much wider area of bulk materials.

Methods

Crystals growth

La(O,F)BiS₂ single crystals were grown by a high-temperature flux method in a vacuumed quartz tube. The raw materials of La₂S₃, Bi, Bi₂S₃, Bi₂O₃, BiF₃ were weighed to have a nominal composition of LaO_{0.4}F_{0.6}BiS₂. A mixture of raw materials (0.8 g) and CsCl/KCl flux (5.0 g) with a molar ratio of 5:3 was combined using a mortar, and then sealed in a quartz tube under vacuum. The quartz tube was heated at 800 °C for 10 h, cooled slowly to 600 °C at a rate of 1 °C/h, and then furnace-cooled to room temperature. The quartz tube was opened in air, and the flux was dissolved in the quartz tube using distilled water. LaO_{0.55}F_{0.45}BiS₂ single crystals were obtained in this product. The obtained single crystals had good cleavage, producing flat surfaces as large as ~ 1x1 mm².

Angle-resolved photoemission spectroscopy (ARPES) and Spin- and angle resolved photoemission spectroscopy (SARPES)

Both ARPES and SARPES measurements were performed at ESPRESSO endstation²⁵ of Hiroshima Synchrotron Radiation Center (HiSOR). The VLEED-type spin polarimeter utilized in the ESPRESSO achieves a 100 times higher efficiency compared to that of conventional Mott-type spin detectors, which offers a great advantage for high-resolution spin analysis of nonmagnetic system as in present case. The spin polarizations of photoelectrons can be measured by switching the directions of the target magnetizations by coils such that ESPRESSO machine can resolve both out-of-plane (P_z) and in-plane (P_x/P_y) spin polarization components with high angular and energy resolutions²⁶. The sign of the polar (tilt) angle is defined as negative (positive) in the case of anticlockwise rotation about y axis (x axis) as shown in Fig. 1b. The overall experimental energy and wave number resolutions of ARPES (SARPES) were set to 35 meV and < 0.008 Å⁻¹ (60 meV and < 0.04 Å⁻¹), respectively. The samples were cleaved in-situ under ultrahigh vacuum(UHV) below 1 × 10⁻⁸ Pa and the sample temperature was kept at 50 K which is higher than superconducting critical temperature (T_c). In addition, supplemental high-resolution ARPES measurement was performed at the beamline BL9A of HiSOR to check if the crossing of the LCB band can be seen by ARPES or not. The energy and angular resolution were set to 10 meV and < 0.004 Å⁻¹. Samples are cleaved in situ in the UHV chamber at room temperature and measured at 50 K.

References

1. Zhang, X. *et al.* Hidden spin polarization in inversion-symmetric bulk crystals. *Nat. Phys.* **10**, 387-393 (2014).
2. Dresselhaus G. Spin-Orbit Coupling Effects in Zinc Blende Structures. *Phys. Rev.* **100**, 580 (1955).
3. Vervoort, L., Ferreira, R., & Voisin, P. Effects of interface asymmetry on hole subband degeneracies and spin-relaxation rates in quantum wells. *Phys. Rev. B* **56**, R12744 (1997).
4. Ishizaka, K. *et al.* Giant Rashba-type spin splitting in bulk BiTeI. *Nat. Mater.* **10**, 521–526 (2011).
5. LaShell, S., McDougall, B., & Jensen, E. Spin splitting of an Au (111) surface state band observed with angle resolved photoelectron spectroscopy. *Phys. Rev. Lett.* **77**, 3419 (1996).
6. Nitta, J. *et al.* Gate Control of Spin-Orbit Interaction in an Inverted In_{0.53}Ga_{0.47}As/In_{0.52}Al_{0.48}As Heterostructure. *Phys. Rev. Lett.* **78**, 1335-1338 (1997).
7. Ast, C. R. *et al.* Giant spin splitting through surface alloying. *Phys. Rev. Lett.* **98**, 186807 (2007).
8. King, P. D. C. *et al.* Quasiparticle dynamics and spin–orbital texture of the SrTiO₃ two dimensional electron gas. *Nat. Commun.* **5**: 3414 (2014).
9. Liu, Q., Guo, Y. & Freeman, A. J. Tunable Rashba effect in two-dimensional LaOBiS₂ films: Ultrathin candidates for spin field effect transistors. *Nano. Lett.* **13**, 5264–5270 (2013).
10. Liu, Q. *et al.* Search and design of nonmagnetic centrosymmetric layered crystals with large local spin polarization. *Phys. Rev. B* **91**, 235204 (2015).
11. Liu, J. *et al.* Giant superconducting fluctuation and anomalous semiconducting normal state in NdO_{1-x}F_xBi_{1-y}S₂ single crystals. *Europhys. Lett.* **106**, 67002 (2014).
12. Agatsuma, T., & Hotta, T. Fermi-surface topology and pairing symmetry in BiS₂-based layered superconductors. *J. Magn. Magn. Mater.* **400**, 73-80 (2016).
13. Mizuguchi, Y. *et al.* Superconductivity in Novel BiS₂-Based Layered Superconductor LaO_{1-x}F_xBiS₂. *J. Phys. Soc. Jpn.* **81**, 114725 (2012).

14. Gor'kov, L. P. *et al.* Superconducting 2D system with lifted spin degeneracy: Mixed singlet-triplet state. *Phys. Rev. Lett.* **87**, 037004 (2001).
15. Frigeri, P. A. *et al.* Superconductivity without Inversion Symmetry: MnSi versus CePt₃Si. *Phys. Rev. Lett.* **92**, 097001 (2004).
16. Takimoto, T. *et al.* Triplet cooper pair formation by anomalous spin fluctuations in non-centrosymmetric superconductors. *J. Phys. Soc. Jpn.* **78**, 103703 (2009).
17. Cappelluti, E. *et al.* Topological change of the Fermi surface in low-density Rashba gases: application to superconductivity. *Phys. Rev. Lett.* **98**, 167002 (2007).
18. Yang, Y. *et al.* Triplet pairing and possible weak topological superconductivity in BiS₂-based superconductors. *Phys. Rev. B* **88**, 094519 (2013).
19. Dai, C. L. *et al.* Theoretical study of the physical properties of BiS₂ superconductors. *Phys. Rev. B* **91**, 024512 (2015).
20. Qi, X. L., & Zhang, S. C. Topological insulators and superconductors. *Rev. Mod. Phys.* **83**, 1057 (2011).
21. Jha, R. *et al.* Superconductivity at 5 K in NdO_{0.5}F_{0.5}BiS₂. *J. Appl. Phys.* **113**, 056102 (2013).
22. Awana, V. P. S. *et al.* Appearance of superconductivity in layered LaO_{0.5}F_{0.5}BiS₂. *Solid. State. Commun.* **157**, 21-23 (2013).
23. Lee, J. *et al.* Crystal structure, lattice vibrations, and superconductivity of LaO_{1-x}F_xBiS₂. *Phys. Rev. B* **87**, 205134 (2013).
24. Nagao, M. *et al.* Growth and superconducting properties of F-substituted ROBiS₂ (R= La, Ce, Nd) single crystals. *Solid. State. Commun.* **178**, 33-36 (2014).
25. Okuda, T. *et al.* Efficient spin resolved spectroscopy observation machine at Hiroshima Synchrotron Radiation Center. *Rev. Sci. Instrum.* **82**, 103302 (2011).
26. Okuda, T. *et al.* A double VLEED spin detector for high-resolution three dimensional spin vectorial analysis of anisotropic Rashba spin splitting. *J. Electron Spectros. Relat. Phenomena* **201**, 23–29 (2015).
27. Usui, H. *et al.* Minimal electronic models for superconducting BiS₂ layers. *Phys. Rev. B* **86**, 220501 (2012).
28. Terashima, K. *et al.* Proximity to Fermi-surface topological change in superconducting LaO_{0.54}F_{0.46}BiS₂. *Phys. Rev. B* **90**, 220512 (2014).
29. Miyamoto, K. *et al.* Orbital-symmetry-selective spin characterization of Dirac-cone-like state on W (110). *Phys. Rev. B* **93**, 161403 (2016).
30. Riley, J. M. *et al.* Direct observation of spin-polarized bulk bands in an inversion-symmetric semiconductor. *Nat. Phys.* **10**, 835-839 (2014).
31. Wu, S. L. *et al.* Synthesis and physical property characterization of LaOBiSe₂ and LaO_{0.5}F_{0.5}BiSe₂ superconductor. *Solid. State. Commun.* **205**, 14-18 (2015).
32. Dong, X. Y. *et al.* Electrically tunable multiple Dirac cones in thin films of the (LaO)₂(SbSe₂)₂ family of materials. *Nat. Commun.* **6**: 8517 (2015).

Acknowledgements

The experiments were performed with the approval of Proposal Assessing Committee of the Hiroshima Synchrotron Radiation Center (Proposal No. 16AG052 and 16AU004).

S.W., T.O. thank Prof. Hitoshi Sato, Mr. Rousuli Awabakeli, Mr. Ming-Tian Zheng, Dr. Eike Fabian Schwier and Prof. Kenya Shimada for their support during supplemental experiments at beamlines BL7 and BL1 in HiSOR.

Author contribution

S.W., K.S., K.T., T.Y., K.M., M.A. and T.O. carried out ARPES and SARPES measurement. M.N., S.W. and I.T. synthesized and characterized the single crystals. S.W. analyzed (S)ARPES data and wrote the manuscript with input from M.K., Y.U., A.K., and T.O.. T.O. conceived the experiment. All authors contributed to the scientific discussions.

SUPPLEMENTARY INFORMATION — Direct evidence of hidden local spin polarization in a centrosymmetric superconductor $\text{LaO}_{0.55}\text{F}_{0.45}\text{BiS}_2$

Shilong Wu¹, Kazuki Sumida², Koji Miyamoto¹, Kazuaki Taguchi², Tomoki Yoshikawa², Akio Kimura², Yoshifumi Ueda¹, Masanori Nagao³, Satoshi Watauchi³, Isao Tanaka³, and Taichi Okuda¹

¹Hiroshima Synchrotron Radiation Center (HSRC), Hiroshima University, 2-313 Kagamiyama, Higashi-Hiroshima 739-0046, Japan

²Graduate School of Science, Hiroshima University, 1-3-1 Kagamiyama, Higashi-Hiroshima 739-8526, Japan

³Center for Crystal Science and Technology (CCST), University of Yamanashi, 7-32 Miyamae, Kofu, Yamanashi 400-8511, Japan

Supplementary Note 1. The detailed structure of conduction band.

Previous theoretical studies^{S1,S2,S3} predicted the conduction band (CB) of LaOBiS_2 compounds splits into inner and outer branches along Γ -X-M line because of the local spin polarization. Moreover, two branches cross along X-M line leading to a crossing point which divides CB into upper (I) and lower (II) regions, as shown in Figure S1.

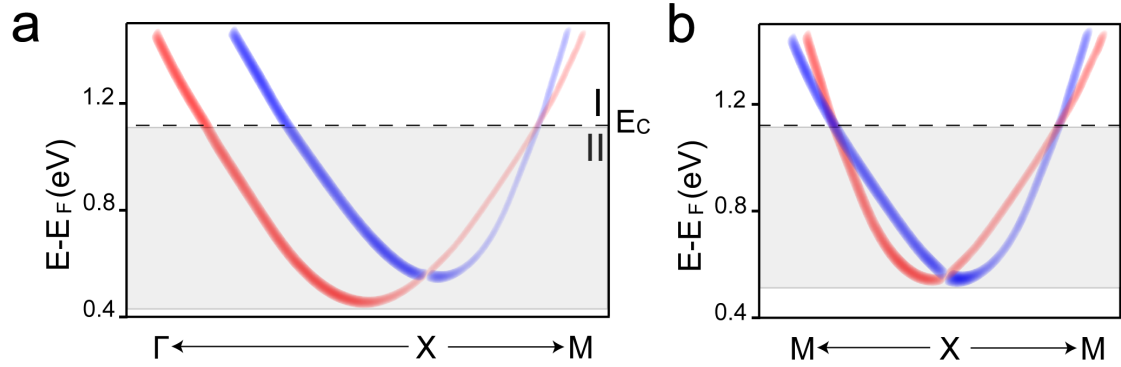


Figure S1. (a) Schematic conduction band (CB) structure around the X point along the Γ -X-M line in LaOBiS_2 parent compounds. A crossing point ($E=E_C$) along X-M line divides the conduction band into upper (I) and lower (II) regions. (b) The same as (a) but along M-X-M line copied from ref. S1 and S2. Note that the binding energy of our ARPES measurement of CB in $\text{LaO}_{0.55}\text{F}_{0.45}\text{BiS}_2$ crystals differs from the calculated bands with around 1.1 eV because of n-type doping effect. The red and blue colors for energy bands represent spin-up and down states, respectively.

Supplementary Note 2. The conversion of R-2 and D-2 spin textures in conduction band.

The crossing structure of CB has profound effect on spin texture^{S1}, Namely, the Rashba-like and Dresselhaus-like spin textures of CECs derived from opposite spin polarizations of upper (I) and lower (II) CB along X-M line^{S1}. The upper band from region I causes the R-2 type helical spin texture while the lower band from region II causes the D-2 type non-helical spin texture, as shown in Figure S2. In the main text we present spectroscopic evidence of this intriguing spin textures of lowest conduction band (LCB) in n-doped $\text{LaO}_{0.55}\text{F}_{0.45}\text{BiS}_2$ superconductor. The charge transfer from adjacent [LaO] blocks to [BiS₂] by fluorine doping realized the metallization of BiS₂ superconducting bilayers^{S4}, which allows us to observe both conduction band and valence band by (Spin-)ARPES measurement.

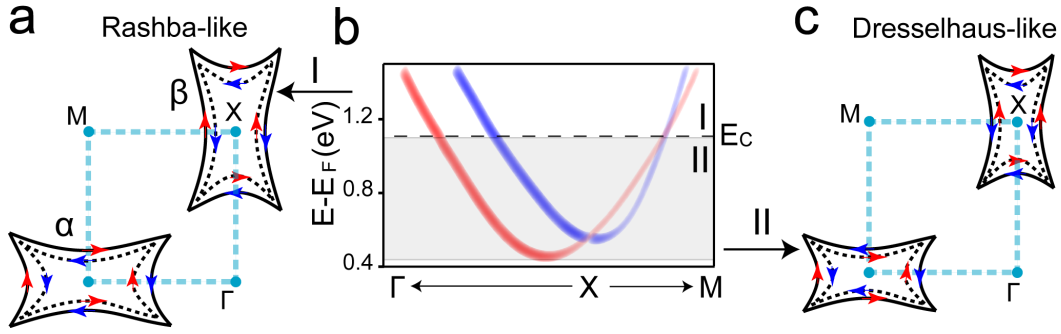


Figure S2. Schematic diagram of spin texture of CB. (a) The Rashba-like spin texture of the rectangle-like shape constant energy contours (CEs) at upper part of CB (region I in S2d). (c) The Dresselhaus-like spin texture of CECs at lower part of CB (region II in S2d) derives from the crossing of spin-polarized CB ($E = E_c$) along X-M line^{S1}. The red and blue colors for arrows and energy bands represent spin-up and down states, respectively.

Supplementary Note 3. Spin-resolved ARPES results of HVB.

We have investigated the spin-polarization of HVB. Fig. S3 presents the spin-resolved EDCs of HVB at positions “c” and “d” and the peaks of spectra are also plotted in the Figure. The results indicate clear spin polarizations at the outer branch of splitting HVB both along Γ -X- Γ and M-X-M lines. Opposite spin polarizations are observed in the binding energy range of the inner branch indicating again the local Rashba spin polarization in HVB.

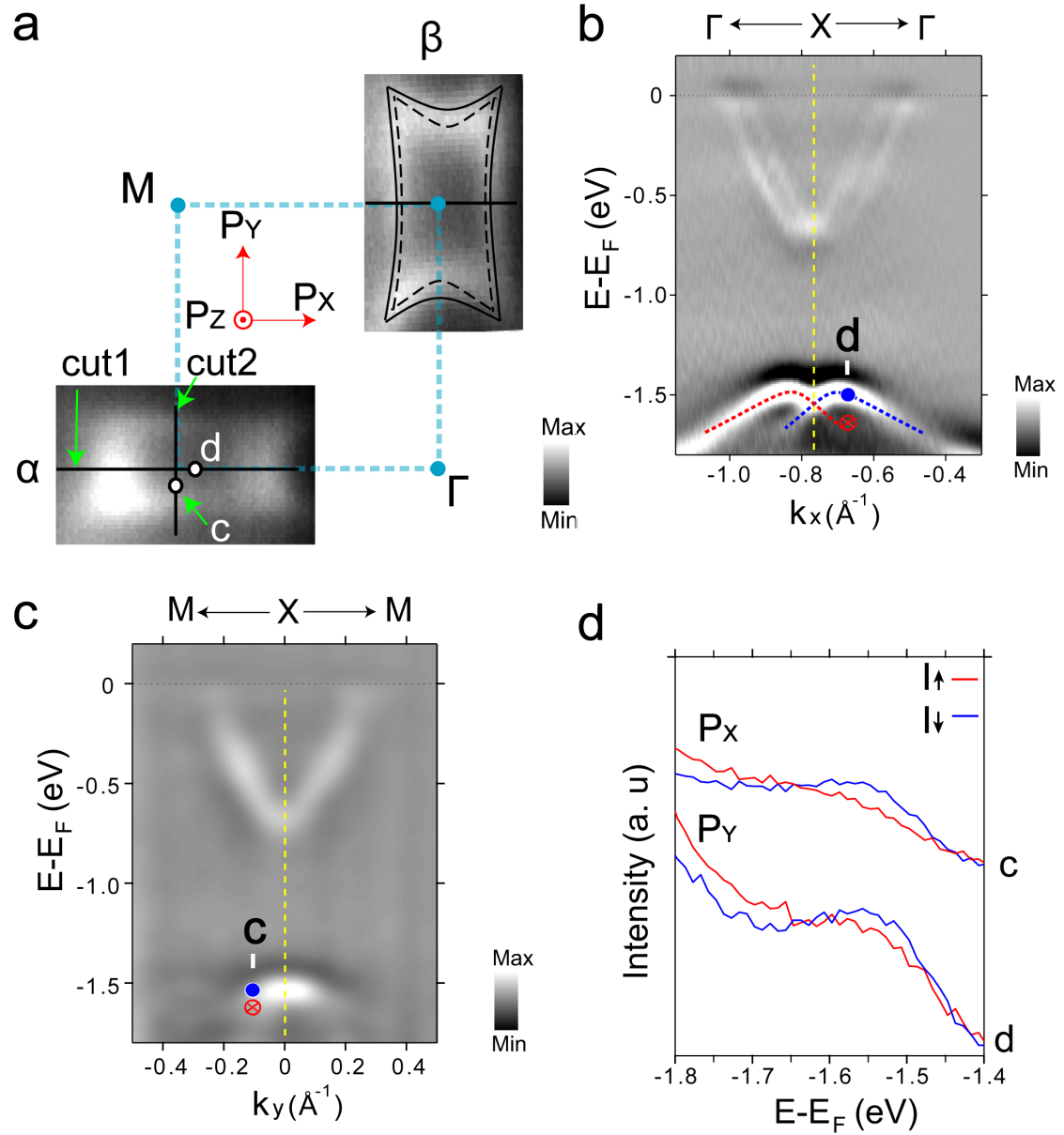


Figure S3. SARPES measurement of highest valence band (HVB). (a) The α and β Fermi surface sheets (FSs) of LCB and the DFT calculation of FSs (black lines). The white dots "c" and "d" around "X" point denote the momentum points where we performed spin measurements in HVB. Coordinate axes (P_x , P_y , P_z) denote positive directions of spin vectors. (b) Band dispersion along the cut 1 (Γ -X- Γ line, second derivative). The dashed red and blue lines represent extracted peak positions from the EDCs used for the estimation of Rashba parameter. (c) Band dispersion along the cut 2 (M-X-M line, second derivative). (d) Spin-resolved EDCs of P_x at point "c" and P_y at point "d" for HVB. The red crosses and blue dots in S3b and S3c stand for spin-up and down states of spin vectors respectively, corresponding to S3d.

Supplementary References

- S1 Zhang, X. *et al.* Hidden spin polarization in inversion-symmetric bulk crystals. *Nat. Phys.* **10**, 387-393 (2014).
- S2 Liu, Q. *et al.* Search and design of nonmagnetic centrosymmetric layered crystals with large local spin polarization. *Phys. Rev. B* **91**, 235204 (2015).
- S3 Liu, Q., Guo, Y. & Freeman, A. J. Tunable Rashba effect in two-dimensional LaOBiS₂ films: Ultrathin candidates for spin field effect transistors. *Nano. Lett.* **13**, 5264–5270 (2013).
- S4 Shein, I. R., & Ivanovskii, A. L. Electronic band structure and Fermi surface for new layered superconductor LaO_{0.5}F_{0.5}BiS₂ in comparison with parent phase LaOBiS₂ from first principles. *JETP Lett.* **96**, 769-774 (2013).